Analyst

Accepted Manuscript

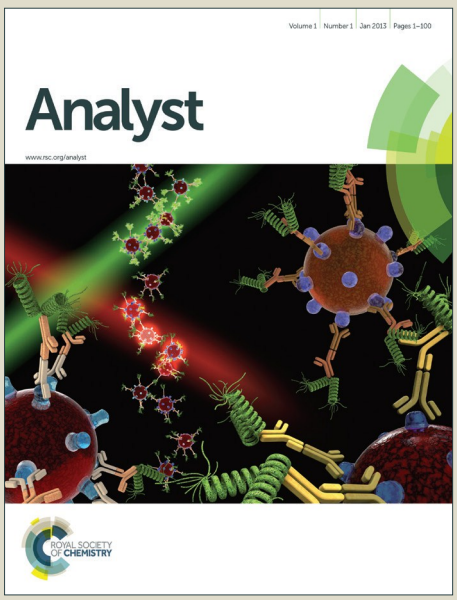

ROYAL SOCIETY OF CHEMISTRY

www.rsc.org/analyst

Journal Name

RSCPublishing

ARTICLE

Tremella-like graphene–Au composites used for amperometric determination of dopamine

Cite this: DOI: 10.1039/x0xx00000x

Cong Li,[a] Jingyu Zhao,[a] Xiaoyi Yan,[a] Yue Gu,[a] Weilu Liu,[a,b] Liu Tang,[a] Bo Zheng,[a] Yaru Li,[a] Ruixue Chen,[a] Zhiquan Zhang [*a]

Received 00th January 2012,
Accepted 00th January 2012

DOI: 10.1039/x0xx00000x

www.rsc.org/

Abstract: Electrochemical detection of dopamine (DA) plays an important role in medical diagnosis. In this paper, tremella-like graphene-Au (t-GN-Au) composites were synthesized by a one-step hydrothermal method for selective detection of DA. Scanning electron microscopy (SEM), X-ray photoelectron spectroscopy (XPS), X-ray diffraction (XRD), Raman spectroscopy, and Fourier transform infrared (FTIR) spectroscopy were used to characterize as-prepared t-GN-Au composites. The t-GN-Au composites were directly used for the determination of DA via cyclic voltammetry (CV) and chronoamperometry (CA) technique. CA measurement gave a wide linear range from 0.8 to 2000 μM, and the detection limit of 57 nM (S/N = 3) for DA. The mechanism and the heterogeneous electron transfer kinetics of the DA oxidation were discussed according to the rotating disk electrode (RDE) experiments. Moreover, the modified electrode was applied to the determination of DA in human urine and serum samples.

1. Introduction

Dopamine (DA) is an electroactive neurotransmitter and plays a vital role in the function of the central nervous system in mammalian.[1] Abnormal levels of DA will lead to neurological disorders, like schizophrenia and Parkinson's disease.[2] Therefore, sensitive and selective determination of DA has an important value in clinical disease diagnosis. Different methods have been used for the determination of DA such as high performance liquid chromatography,[3] fluorescence method,[4] spectrophotometry,[5] and electrochemical method.[6] Nowadays, electrochemical determination of DA has drawn considerable attention due to its simplicity and cost-effectiveness when compared with aforementioned traditional analytical methods.[7] In electrochemical analysis, modified electrodes played an important role for the sensitive and selective detection of DA. Since the bare electrodes have poor sensitivity and selectivity, the oxidation peak potential of DA appeared more positive over potential.[8] So far, various chemically modified electrodes have been fabricated using polymers,[9] metal oxides,[10] nanostructured noble metals,[11] carbon nanostructures,[12] and so on.

For biosensing electrodes, Au nanoparticle is an excellent choice due to its conductivity, stability, biocompatibility and large surface area.[13] For example, Xie et al. fabricated graphene, flower-like zinc oxide, and gold nanoparticles nanocomposite for hydrogen peroxide detection.[14] Xu et al. fabricated flower-like gold nanoparticles/reduced graphene oxide composite, and it showed superior catalytic performance for oxygen reduction reaction.[15] Among various carbon-based materials, graphene oxides (GO) and graphene (GN) have attracted much more attentions due to their high electrical conductivity, excellent mechanical strength, large unit surface area, and high transparency.[14] However, the π-π interaction of GN sheets makes the aggregation and stacking emergence,[15] which decreases the electrolyte diffusion, compromises the specific surface area, and damages the catalyst performance.[16] In order to overcome this problem, synthesizing three-dimensional (3D) GN is a method to be adopted widely. For example, Wang et al.[2] fabricated a flower-like GN electrode using a simple electrochemical method for the detection of DA. Yuan et al.[17] prepared bimetallic Pd-Cu nanoparticle decorated 3D GN hydrogel for glucose detection. Lin et al.[18] reported a 3D activated reduced GO nanocup/nickel aluminum layered double hydroxides composite, and found that it exhibited high electrochemical and capacitance performances. Kung et al.[19] developed a 3D GN foam supported Pt-Ru bimetallic nanocatalysts for hydrogen peroxide detection. Claussen et al. presented Pt nanoparticles on multilayered grapheme petal nanosheets for glucose detection.[22]

Herein, we report a general hydrothermal approach for one-step synthesis of tremella-like graphene (t-GN) decorated with Au nanoparticles, using a GO-$HAuCl_4$/H_2SO_4 aqueous suspension as the precursor and H_2SO_4 as promoting agent. The fabricated electrode showed a good selective detection of DA with high sensitivity. The

proposed method was applied to determination of DA in human urine and serum samples with good selectivity and high sensitivity.

2. Experimental

2.1. Apparatus

The electrode materials were characterized by Scanning electron microscopy (SEM, Hitachi S-4800), X-ray photoelectron spectroscopy (XPS, AlKα radiation, ESCALAB-MKII 250 photoelectron spectrometer, VG Co.), X-ray diffraction (XRD, CuKα radiation, D/max2550VB X-ray diffractometer, Rigaku), Raman spectroscopy (solid-state laser at 633nm radiation, Renishaw inVia Raman Microscope, UK), and Fourier transform infrared spectroscopy (Nicolet Impact 410 FTIR spectrometer). Cyclic voltammetry (CV) and chronoamperometry (CA) methods were utilized to examine the electrochemical sensing properties of t-GN-Au composites towards DA. All electrochemical measurements were carried out on a CHI920C electrochemical workstation (Shanghai Chenhua). A conventional three-electrode system was employed with a bare or modified glassy carbon electrode (GCE, 3 mm diameter) as working electrode, a platinum wire as the counter electrode, a saturated calomel electrode (SCE) as the reference electrode. Rotating disk electrode (RDE) experiments were performed on a BAS RDE-2 electrode by linear sweep voltammetry (LSV) at a potential sweep rate of 5 mV s^{-1}. All potentials reported in this paper were referenced to the SCE.

2.2. Chemicals and materials

Natural graphite was purchased from Qingdao Hengrui Industrial, China. Chloroauric acid ($HAuCl_4$) was obtained from Shanghai Chemical Reagent Factory. (Shanghai, China). DA was purchased from Aladdin. The 0.04 M Britton-Robinson (BR) buffer solution was prepared by mixing a solution of 0.04 M in phosphoric acid (H_3PO_4), 0.04 M in acetic acid and 0.04 M in boric acid (H_3BO_3) with the appropriate amount of 0.2 M sodium hydroxide solution. All reagents were of analytical grade and used without further purification. Doubly distilled water was used in this experiment throughout. Human urine samples were provided by a healthy volunteer. The human blood samples were collected from First Hospital, Jilin University, Changchun. The blood, treated with ethylene diamine tetraacetic acid (EDTA) as an anticoagulant, was centrifuged at 3000 rpm. After 30 min, three phases appeared. The upper phase (blood plasma) was separated and was fractionated by further centrifugation at 9000 rpm for 30 min. The supernatant blood plasma was used to determine the DA concentration.

2.3. Preparation of the modified electrode

First, graphene oxide (GO) was synthesized from natural graphite powder by the modified Hummers method,[20] and the 5 mg GO was dissolved in 5 mL doubly distilled water to form a homogeneous solution. 2 mL of 0.5 mM $HAuCl_4$ water solution was subsequently added, drop by drop, to the GO solution, and the solution was sonicated for 15 min. Then, 280 μL concentrated H_2SO_4 (98%) was added to the aqueous suspension. After being homogenized by stirring for several minutes, a total of 7 mL GO/H_2SO_4 aqueous suspension was transferred to a 20 mL Teflon-lined autoclave and heated at 160 °C for 10 h. The resultant t-GN-Au composites were recovered by filtration, washed with doubly distilled water for several times and dried at 50 °C in air for 10 h. For comparison, the layer-stacking GN-Au composites were prepared according to the literature and described in the supporting information (ESI†).[21] Prior to modification, the bare GCE was polished successively with 0.3 and 0.05 μm Al_2O_3 slurry on the tracing paper. Then it was washed successively with 1:1 nitric acid, ethyl alcohol, and water in an ultrasonic bath and dried under a stream of nitrogen. Afterwards, 7.5 μL of t-GN-Au or GN-Au suspension (1 mg mL^{-1}) was carefully cast on the cleaned GCE surface.

3. Results and discussion

3.1. Characterization of composites

It has been reported that the polymerization and carbonization of glucose solution under hydrothermal condition could be acid-catalyzed.[22] This process is accompanied with formation of gaseous products (CO_2, CO and H_2). GO sheets share similar functional groups (hydroxyl, and carbonyl) with glucose molecules, so these bubbles can be generated in the GO aqueous suspension under hydrothermal conditions.[23] However, GO with negatively charged attract Au^{3+} via the electrostatic interactions, which makes bubbles decrease. After adding H_2SO_4 to GO-$HAuCl_4$ aqueous suspension, GO sheets prefer to aggregate around the liquid/gas interface.[24] So it could form tremella-like structure. Fig. 1A showed SEM images of the t-GN-Au. As can be seen, the t-GN-Au composites presented a tremella-like structure. From the insert of Fig. 1A, it was observed that Au nanocrystals grew on the surface of t-GN successfully, which confirmed the formation of t-GN-Au composites.

The obtained composites were also characterized by XRD (Fig. 1B). After hydrothermal process, the diffraction peak of exfoliated GO at 2θ = 10.9° disappeared and a very broad peak around 24.3° was observed in the t-GN-Au sample, indicating that most oxygen functional groups had been removed. Also, the peaks found at 2θ = 38.2°, 44.4°, 64.6°, and 77.6° were assigned to the Au (111) (200) (220) (311) face, respectively, showing the formation of gold nanoparticles.[25] Raman spectroscopy is a nondestructive approach to characterize graphitic materials, in particular to determine ordered and disordered crystal structures of GN.[26] Fig. 1C presented typically Raman spectra of the GO, GN, and t-GN-Au. For three

Journal Name RSCPublishing

ARTICLE

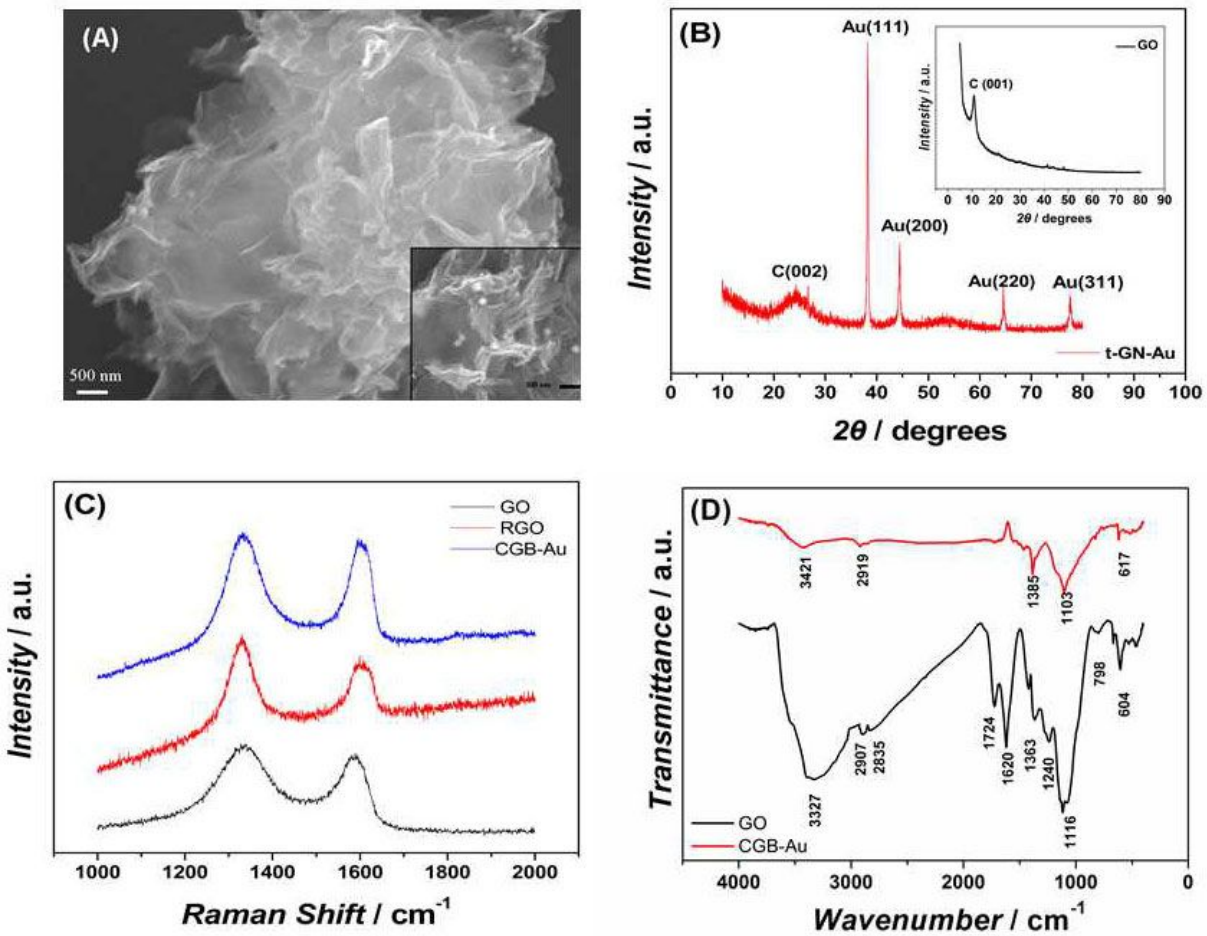

Fig. 1 (A) SEM image of as-prepared t-GN-Au. Insert: corresponding to the high magnified SEM image. (B) XRD patterns of t-GN-Au. Insert: XRD patterns of GO. (C) Raman spectroscopy of GO, GN, and t-GN-Au. (D) FTIR spectroscopy of GO and t-GN-Au.

materials, there were two prominent peaks on the Raman spectra, including D band (1330 cm^{-1}) and G band (1598 cm^{-1}). The D/G intensity ratio can be used to predict the amount of defects within the GN samples. Compared with D/G intensity ratio of GO (1.06), GN (1.24) and t-GN-Au (1.16), which indicated that a good reduction degree of GN and t-GN-Au, and that the formation of t-GN-Au did not destroy the intrinsic structural property of GN sheets. Fig. 1D showed the FTIR transmittance spectra of GO and t-GN-Au composites. The characteristic vibration was the broad and intense peak of O-H groups centered at 3377 cm^{-1}. The peaks at 2907 and 2835 cm^{-1} were designated as the asymmetric and symmetric stretching vibrations of methyl and methylene groups. The adsorption bands at 1724 and 1116 cm^{-1} were assigned to the C=O and C-O (alkoxy) stretching vibrations, respectively, which suggest the successful oxidation of graphite.[27] It was worth noting that, after hydrothermal process, the intensities of the peaks decreased significantly and some peaks of oxygen functional groups disappeared. This proved the reduction of GO.

The surface states of t-GN-Au were investigated by XPS measurements. For the C 1s spectra, the C-O bonds were the main species for GO (Fig. S1A in the ESI†), while the C-C bonds became predominant for t-GN-Au after hydrothermal reaction (Fig. S1B). It revealed the efficient reduction of oxygenous groups on GO.[28, 29] As shown in the insert of Fig. S1B, the resulting nanohybrid showed a significant Au 4f binding energy consistent with zero-valent Au.[30] It confirmed the formation of Au nanocrystals coated on the t-GN.

3.2. Electrochemical behavior of DA on the t-GN-Au/GCE

The electrochemical response of DA at the GCE, the GN-Au/GCE, and the t-GN-Au/GCE was examined using CV in a 300 μM DA solution (pH 6.0). As shown in Fig. 2, at the bare GCE (dotted line), DA showed a pair of irreversible and relatively weak redox peaks at 0.392 V (E_{pa}) and 0.057 V (E_{pc}). The potential difference of the redox peaks was 0.335 V. At the GN-Au/GCE (dashed line), the oxidation peak current increased by a factor of 2.67 compared with the bare GCE. When the t-GN-Au was fixed on the GCE surface, DA exhibited the largest oxidation peak current, (solid line), which was 5.30 times higher than that on the bare GCE, and the potential difference was decreased to 0.240 V. The redox peaks increased obviously, benefiting from the unique tremella-like structure of the t-GN-Au, which can provide more active area for the oxidation of DA. The tremella-like GN together with Au nanoparticle introduced an obviously sensitized effect toward the electrochemical redox of DA. Meanwhile, the t-GN-Au with a negative charge, which not only provided good stability but also enabled interaction with DA through electrostatic interaction to recognize DA with high specificity.

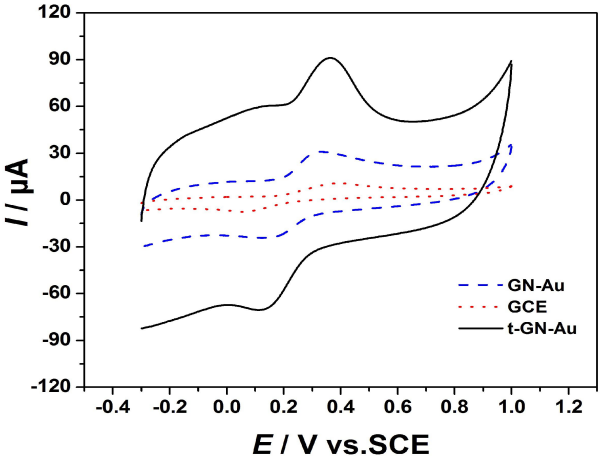

Fig. 2 Cyclic voltammograms of 300 μM DA in BR buffer solution (pH 6.0) at the bare GCE (dotted line), the GN-Au modified GCE (dashed line), and the t-GN-Au modified GCE (solid line). The potential scan rate is 100 mV s^{-1}.

3.3. Effect of the potential scan rate

The influence of scan rate on the peak currents of 300 μM DA in 0.04 M BR buffer solution at the t-GN-Au/GCE was investigated by CV (Fig. S2 in the ESI†). As shown in Fig. S2B, a good linear relationship between the peak current and the square root of the scan rate ($v^{1/2}$) from 50 to 470 mV s^{-1} was obtained. The regression equation was I_{pa} (μA) = 5.728 $v^{1/2}$ (mV s^{-1})$^{1/2}$ – 20.96 (R=0.999). This demonstrated that the redox process of DA at the t-GN-Au/GCE was controlled by diffusion.

3.4. Optimization of the conditions

3.4.1 Effect of the amount of t-GN-Au on the modified GCE

The oxidation current of DA at the prepared sensor can be affected by the amount of modifier on the electrode surface. Fig. 3 showed a plot of the anodic peak current for DA *versus* the volume of the dropped suspension. Clearly, it can be observed that 7.5 μL of the suspension showed the best current response to DA. When the dropped suspension was less than 7.5 μL, the formed film was hard to cover the electrode surface with 3 mm in diameter, which was not enough to obtain the optimal response to DA. However, as the volume of the suspension increased to 10 μL, the formed film becomes too thick, which would be unfavorable not only for the electron transfer but also for the diffusion of DA to the modified electrode, leading to a lower response. As a result, 7.5 μL of suspension was selected as the optimum amount for preparation of the modified electrode.

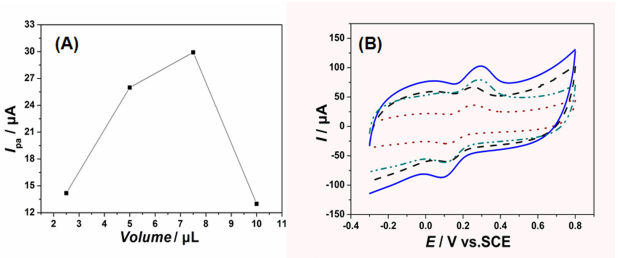

Fig. 3 (A) Plot of anodic peak current for DA *versus* volume of the dropped suspension. (B) Cyclic voltammograms of 300 μM DA in BR buffer solution for different volumes of the dropped suspension (2.5 μL correspond to dotted line, 5 μL correspond to dash dot dotted line, 7.5 μL correspond to solid line, and 10 μL correspond to dashed line).

3.4.2 Effect of solution pH

The effect of pH value on the electrochemical behavior of 300 μM DA in 0.04 M BR buffer solution at the t-GN-Au/GCE was carefully investigated by CV in the pH range from 4.0 to 10.0 (Fig. 4A). The insert of Fig. 4B revealed that the largest peak current was obtained at pH 6.0. Therefore, pH 6.0 was chosen as the optimum pH value for the detection of DA in order to achieve high sensitivity. In addition, the relationship between pH and the anodic peak potential was investigated (Fig. 4B). It was observed that the anodic peak potentials of DA shifted to more negative with the increase of pH in the range of pH 4.0-10.0. The equations for peak potential with pH for DA E_{pa} (mV) = -60.64 pH + 758.8 (R=0.997). The slope is 60.64 mV pH^{-1}, which is very close to the Nernstian value of 59 mV pH^{-1} at 25 ℃. According to the equation: -59m/n = -60.64, where n is the transferred electron number and m is the number of hydrogen ions participating in the reaction, the number of transferred electrons was equal with that of hydrogen ions taking part in the electrode reaction.[31]

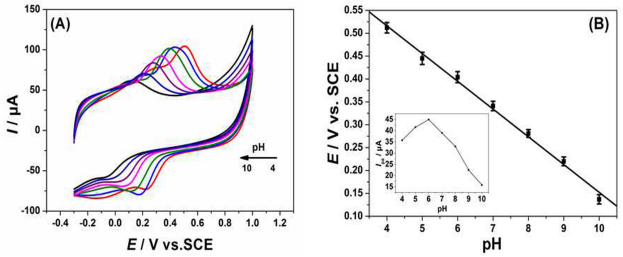

Fig. 4 (A) Cyclic voltammograms of 300 μM DA at the t-GN-Au modified GCE in BR buffer solution with different pH values (4.0-10.0). Scan rate: 100 mV s^{-1}. (B) Plot of peak potential for DA *versus* pH values. Insert: Plot of anodic peak current for DA *versus* pH values (error bars show SD of three measurements).

3.4.3 Optimization of instrumental parameters

To study the effect of applied potentials on electrocatalytic oxidation of DA at the t-GN-Au/GCE, the amperometric responses of the t-GN-Au/GCE to four successive injection of 10 μM DA were recorded at various applied potentials (Fig. 5). The t-GN-Au/GCE exhibited sensitive and rapid current response to the DA addition, achieving steady state current in less than 5 s. The sensitivity was higher at the applied potential of 0.40 V compared to that at 0.35 V and 0.45 V. Thus 0.40 V was chosen as the working potential in the quantification experiments.

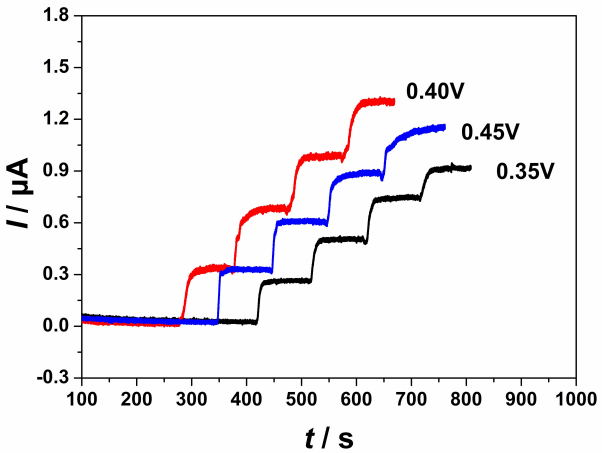

Fig. 5 (A) The amperometric responses of the electrode to four successive injection of 10 μM DA at the t-GN-Au/GCE at different applied potentials.

3.5. Rotating disk electrode investigation

RDE is a powerful technique to investigate the mechanism and kinetics of electrode reactions.[32] Fig. 6 showed the RDE response of 300 μM DA at the modified electrode under the rotation speeds from 600 rpm to 4200 rpm. Steady-state character of the measured currents was ensured by controlling the sweep rate at 5 mV s^{-1}. In the inset (A) of Fig. 6, the Levich plots (I versus $\omega^{1/2}$) under different electrode potentials were found to be deviated from the straight line, indicating that a kinetic limitation is involved in the electron-transfer reaction. In this case, the current of the electrode reaction can be estimated by the Koutecky-Levich equation.[33]

$$I^{-1} = I_{Lev}^{-1} + I_K^{-1}$$

where, I_{Lev} is the Levich current, I_K is the kinetic current. It can be defined by

$$I_{Lev} = 0.62nFAD^{2/3}\upsilon^{-1/6}\omega^{1/2}C_o$$

$$I_K = nFAC_ok$$

where n is the number of electron transferred, F (96485.3 C mol^{-1}) is the Faraday constant, A (0.131 cm^2) is the electrochemical active electrode area, which was calculated by chronoamperometry using a solution containing 1 mM $Fe(CN)_6^{3-}$ and 0.1 M KCl according to the Conttrell equation.[34] D (6.3×10^{-6} cm^2 s^{-1}),[35] υ (0.01 cm^2 s^{-1}) is the kinematic viscosity, ω (rad s^{-1}) is the rotation rate and k (cm s^{-1}) is the heterogeneous electron transfer rate constant. C_o is the bulk concentration (M).

The insert (B) of Fig. 6 exhibit the Koutecky-Levich plots (I^{-1} versus $\omega^{-1/2}$) constructed at the electrode potentials of 0.45V, 0.5V, 0.55V, and 0.6V, respectively. By measuring the slope of the Koutecky-Levich plots, the average number of electron transfer was calculated to be 2.20. Thus, the oxidation of DA at t-GN-Au is probably to be a two-electron electrode process, which is consistent with the previous reports.[36] By measuring the intercept of the curves in the Koutecky-Levich plots, the heterogeneous electron transfer rate constants at the potential of 0.45V, 0.5V, 0.55V, and 0.6V were calculated as 5.46×10^{-3}, 6.91×10^{-3}, 9.03×10^{-3}, and 1.12×10^{-2} cm s^{-1}, respectively. These kinetic parameters should be useful for the further development of high-performance DA oxidation catalysts.

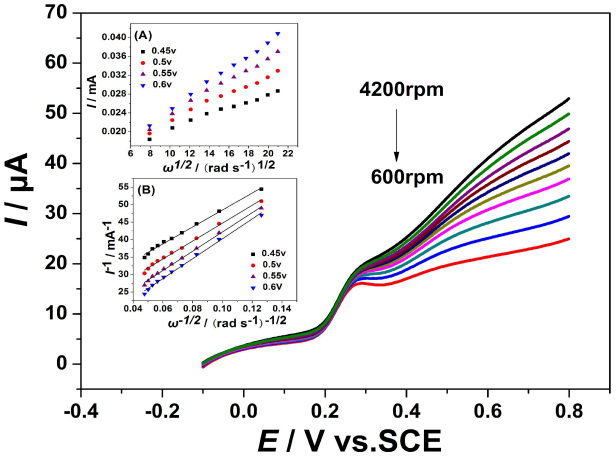

Fig. 6 RDE polarization curves at the t-GN-Au modified GCE in BR buffer solution (pH 6.0) containing 300 μM DA. Potential scan rate: 5 mV s^{-1}. The electrode rotation rates from top to bottom are 4200, 3800, 3400, 3000, 2600, 2200, 1800, 1400, 1000, 600 rpm, respectively. The inserts are Levich plots (A) and Koutecky-Levich plots (B) at different electrode potentials.

3.6. Calibration plot and limit of detection

Using the optimized experimental conditions described above CA was carried out to evaluate the analytical performance of t-GN-Au/GCE in quantification of DA. Fig. 7A showed the chronoamperometric response of the t-GN-Au/GCE at 0.40 V upon successive addition of different concentrations of DA (0.8, 5, 10, 50, 100, 200, 400, 600, 800, 1000, 1500, 2000 μM) to a pH 6.0 BR buffer solution under continuous stirring. The current increased and reached the steady value rapidly when DA was added into the BR buffer solution. The response time was less than 5 s. Fig. 7B showed the calibration curve based on the oxidation current responses which revealed that the modified electrode had a linear response to DA in the range of 0.8 to 2000 μM, with a detection limit of 57 nM (S/N = 3) and a correlation coefficient of 0.9974. The sensitivity of the electrode was 200.6 μA mM^{-1} cm^{-2}. The linear response range was wider, and the detection limit was lower than previous reports. [11, 37-42] It can be attributed to the fact that the t-GN-Au/GCE with tremella-like structure can provide more active area for the oxidation of DA.

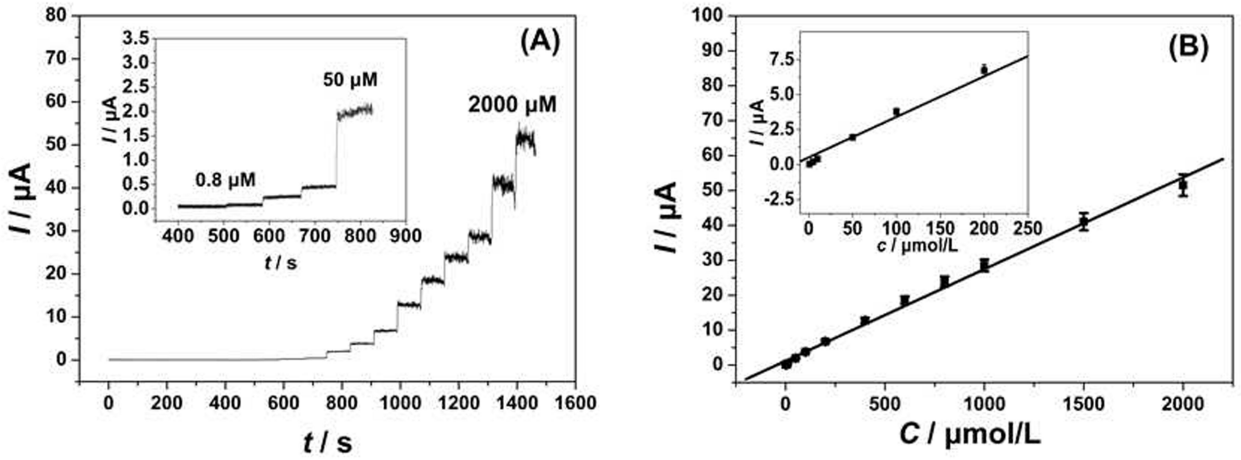

Fig. 7 Amperometric current-time curve of different concentrations of DA in BR buffer solution (pH 6.0) at the t-GN-Au modified GCE using a working potential of 0.40 V, from bottom to top, 0.8, 5, 10, 50, 100, 200, 400, 600, 800, 1000, 1500, 2000 μM (A), and the corresponding calibration curve (B) (error bars show SD of five measurements).

3.7. Selectivity, repeatability, stability and interferences

Selectivity is a very important aspect of sensor performance. As we know, using a bare GCE, the oxidation peak potentials for ascorbic acid (AA), uric acid (UA) and DA are very close to each other and thus it is difficult to separate these compounds due to their overlapping signals[43]. Catechol (CT) and epinephrine (EP) molecules also have the vicinal diols structure. In order to examine the ability of the t-GN-Au/GCE to selectively detect DA, the electrochemical behavior of 1200 μM of AA, 300 μM of DA, 300 μM of UA, 300 μM of CT, and 300 μM of EP at the t-GN-Au/GCE were investigated by CV. As shown in Fig. 8A, the anodic peak current of DA at the t-GN-Au/GCE was greatly improved. However, the responses of UA, AA, EP, and CT at the t-GN-Au/GCE were weakened, as described in Fig. 8B-E. According to the change of the peak current shown in Fig. 8F, the response on the t-GN-Au/GCE toward DA was about 5.30 fold greater than that at the bare GCE. However, the responses of AA, UA, EP, and CT were weaker relative to that at the bare GCE. This was attributed to the electrostatic interaction between the modifier and the analytes. In the pH 6.0 BR buffer solution, both AA (pKa = 4.1) and UA (pKa = 5.75) are negatively charged, but DA (pKa = 8.89) is positively charged.[44, 45] Consequently, DA is attracted and accumulated by the negative charges at the t-GN-Au/GCE. Both AA and UA, which are negatively charges, are repelled by t-GN-Au/GCE. Although CT (pKa = 9.45) and EP (pKa = 8.59) are positively charged, there are amine functional groups in the DA molecules, which could enable the reaction with carboxyl groups in t-GN-Au to recognize DA with high specificity.[46]

The modified electrode presented a good repeatability and durability. The relative standard deviation (RSD) of the peak current is 1.53% for ten continuous measurements of 300 μM DA with the same electrode. The peak currents remain 92.1% of their initial values for determination of 300 μM DA after the modified electrode was kept for ten days at room temperature. The possible interferences of some ions were also investigated. The results show that 100-fold concentration of K^+, Na^+, Ca^{2+}, Zn^{2+}, Li^+, Cu^{2+}, Cl^-, $H_2PO_4^-$, HPO_4^{2-}, NO_3^-, SO_4^{2-}, ClO_4^-, glucose, 50-fold concentration of riboflavin and folic acid, and 5-fold concentration of uric acid and ascorbic acid have no effect on determination of DA (5.0 μM).

3.8. Analytical applications

An investigation into the effect of the pH of the electrolyte solution on the peak current was carried out by CV using the modified electrode in a mixture of BR buffer solution and real samples of different pH, containing 300 μM DA. 10 μL aliquots of urine samples or serum samples were added to the electrochemical cell containing BR buffer solution (pH 4.0–10.0) with 300 μM DA. The results were shown in Fig. S3A and B, as can be seen, the oxidation

peak current for DA was highest at pH 6.0 and decreased gradually with increasing pH, which was consistent with previous results. It could be concluded that the modified electrode presented good repeatability and stability in real samples. Consequently, a BR buffer solution of pH 6.0 was selected as the supporting electrolyte in analytical application.

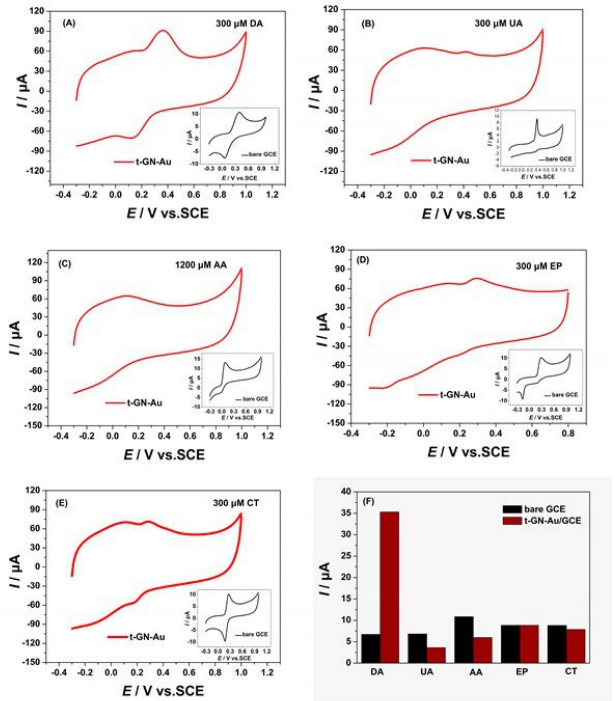

Fig. 8 Cyclic voltammograms of bare GCE (insert black line) and t-GN-Au/GCE (red line) toward different analytes: (A) DA (300 μM), (B) AA (1200 μM), (C) UA (300 μM), (D) EP (300 μM), (E) CT (300 μM); (F) columns of peak currents for different analytes at the bare GCE and t-GN-Au/GCE, respectively.

Quantification of DA in the human urine and serum samples was performed to evaluate the applicability of the proposed system. In this study, the determination of DA was performed in quintuplicate, using the standard addition method. 10 μL aliquots of urine samples or serum samples were added to the electrochemical cell containing BR buffer solution (pH 6.0). No DA was detected, which could be explained either by the absence of DA in the urine and serum sample or that any DA present were below the detection limit of the electrode. After spiking the urine or serum samples with known concentrations of DA, it was observed chronoamperometric response to DA. The amounts of DA in the human spiked urine and serum samples were determined by the calibration curve, and the results were summarized in Table 1. The developed sensor showed recoveries in the range of 98.96%-102.5% and RSD in the range of 1.45%-3.22%. This clearly indicated that the proposed method should be reliable and effective for DA determination.

Table 1 Recovery of the proposed sensor in real samples

Sample	Added (μM)	Found[a] (μM)	RSD (%)	Recovery (%)
Urine 1	10.00	10.19	1.45	101.9
Urine 2	100.0	98.96	2.83	98.96
Serum 1	10.0	10.25	1.57	102.5
Serum 2	100.0	98.99	3.22	98.99

[a] Average of five determinations

Conclusions

In this work, a one-step strategy for the preparation of t-GN-Au composites was established based on the hydrothermal method, using a GO-$HAuCl_4$/H_2SO_4 aqueous suspension as the precursor and H_2SO_4 as promoting agent. This method, can be carried out in an aqueous medium and does not need expensive equipment like the chemical vapor deposition technique or a toxic reducing agent frequently required by chemical reduction of GO. Therefore, it is fast, simple, cheap, eco-friendly, easy controllable, and readily scalable to industrial levels. The t-GN-Au/GCE displayed higher electrochemical response to DA than that of the layer-stacking GN-Au, which was attributed to more active area of t-GN-Au, and it was specific to DA. We have demonstrated the application of t-GN-Au composites in the amperometric determination of DA with good stability, wide linear range, and low detection limit. Furthermore, this method has been proven applicable in human urine and serum samples. Therefore, the t-GN-Au introduced here is a good candidate to develop electrochemical sensors for the sensitive and selective detection of DA.

Acknowledgements

This work was supported by the National Natural Science Foundation of China (No. 21375045) and Natural Science Foundation of Jilin Province (No. 20130101118JC).

Notes and references

[a] College of Chemistry, Jilin University, Changchun 130012, People's Republic of China.
[b] School of Pharmacy, Shenyang Pharmaceutical University, Shenyang 110016, People's Republic of China
* e-mail: zzq@jlu.edu.cn
Electronic Supplementary Information (ESI) available: [details of any supplementary information available should be included here]. See DOI: 10.1039/b000000x/

1. S. Ku, S. Palanisamy and S. M. Chen, *J. Colloid Interface Sci.*, 2013, **411**, 182-186.
2. H. Wang, F. Ren, R. Yue, C. Wang, C. Zhai and Y. Du, *Colloids. Surf., A*, 2014, **448**, 181-185.
3. F. C. Cheng, Y. Shih, Y. J. Liang, L. L. Yang and C. S. Yang, *J.*

Chromatogr., B: Biomed. Appl., 1996, **682**, 195-200.
4. Q. Mu, H. Xu, Y. Li, S. Ma and X. Zhong, *Analyst*, 2014, **139**, 93-98.
5. Q. Li, J. Li and Z. Yang, *Anal. Chim. Acta*, 2007, **583**, 147-152.
6. X. Zhang, S. Gu and Y. Ding, *Anal. Methods.*, 2014, **6**, 3316-3321.
7. D. Yu, Y. Zeng, Y. Qi, T. Zhou and G. Shi, *Biosens. Bioelectron.*, 2012, **38**, 270-277.
8. F. Chatraei and H. R. Zare, *Anal. Methods.*, 2012, **4**, 2940-2947.
9. Y. Wu, L. Cui, Y. Liu, G. Lv, T. Pu, D. Liu and X. He, *Analyst*, 2013, **138**, 1204-1211.
10. D. Wu, Y. Li, Y. Zhang, P. Wang, Q. Wei and B. Du, *Electrochimica Acta*, 2014, **116**, 244-249.
11. J. Li, J. Yang, Z. Yang, Y. Li, S. Yu, Q. Xu and X. Hu, *Anal. Methods.*, 2012, **4**, 1725-1728.
12. S. Cheemalapati, S. Palanisamy, V. Mani and S. Chen, *Talanta*, 2013, **117**, 297-304.
13. Q. Huang, H. Zhang, S. Hu, F. Li, W. Weng, J. Chen, Q. Wang, Y. He, W. Zhang and X. Bao, *Biosens. Bioelectron.*, 2014, **52**, 277-280.
14. L. L. Xie, Y. D. Xu and X. Y. Cao, *Colloids and Surfaces B:Biointerfaces*, 2013, **107**, 245-250.
15. S. Xu, L. Yong and P. Wu, *Appl. Mater. Interfaces*, 2013, **5**, 654-662.
16. Y. J. Yang and W. Li, *Biosens. Bioelectron.*, 2014, **56**, 300-306.
17. P. Sharma, G. Darabdhara, T. M. Reddy, A. Borah, P. Bezboruah, P. Gogoi, N. Hussain, P. Sengupta and M. R. Das, *Catalysis Communications*, 2013, **40**, 139-144.
18. M. Yuan, A. Liu, M. Zhao, W. Dong, T. Zhao, J. Wang and W. Tang, *Sensor and Actuators B: Chemical*, 2014, **190**, 707-714.
19. M. Yuan, A. Liu, M. Zhao, W. Dong, T. Zhao, J. Wang and W. Tang, *Sens. Actuators, B*, 2014, **190**, 707-714.
20. Y. Lin, L. Ruiyi, L. Zaijun, L. Junkang, F. Yinjun, W. Guangli and G. Zhiguo, *Electrochem. Acta*, 2013, **95**, 146-154.
21. C. C. Kung, P. Y. Lin, F. J. Buse, Y. Xue, X. Yu, L. Dai and C. C. Liu, *Biosens. Bioelectron.*, 2014, **52**, 1-7.
22. J. C. Claussen, A. Kumar, D. B. Jaroch, M. H. Khawaja, A. B. Hibbard, D. M. Porterfield and T. S. Fisher, *Adv. Funct. Mater.*, 2012, **22**, 3399-3405.
23. B. W. S. Hummers, J. R. and R. E. Offeman, *Journal of American Chemical Society*, 1958, **80**, 1339.
24. X. Liu, X. Wang, P. He, L. Yi, Z. Liu and X. Yi, *Journal of Solid State Electrochemistry*, 2012, **16**, 3929-3937.
25. X. Sun and Y. Li, *Journal of Colloid and Interface Science*, 2005, **291**, 7-12.
26. J. Cao, Y. Wang, P. Xiao, Y. Chen, Y. Zhou, J. H. Ouyang and D. Jia, *Carbon*, 2013, **56**, 383-391.
27. Y. Chen, F. Guo, A. Jachak, S. P. Kim, D. Datta, J. Liu, I. Kulaots, C. Vaslet, H. D. Jang, J. Huang, A. Kane, V. B. Shenoy and R. H. Hurt, *Nano*, 2011, **12**, 1996-2002.
28. M. Coros, A. R. Biris, F. Pogacean, L. B. Tudoran, C. Neamtu, F. Watanabe, A. S. Biris and S. Pruneanu, *Electrochem. Acta*, 2013, **91**, 137-143.
29. F. Tuinstra and J. L. Koenig, *The Journal of Chemical Physics*, 1970, **53**, 1126-1130.
30. R. Ojani, R. Valiollahi and J. B. Raoof, *Appl. Surf. Sci.*, 2014, **311**, 245-251.
31. J. Lv, S. Li, A. Wang, L. Mei, J. Chen and J. Feng, *Electrochem. Acta*, 2014, **136**, 521-528.
32. Q. Zhang, Q. Ren, Y. Miao, J. Yuan, K. Wang, F. Li, D. Han and L. Niu, *Talanta*, 2012, **89**, 391-395.
33. J. Chen, X. Cui, Q. Wang, H. Wang, X. Zheng, C. Liu, T. Xue, S. Wang and W. Zheng, *J. Colloid Interface Sci.*, 2012, **383**, 140-147.
34. G. Zheng, M. Chen, X. Liu, J. Zhou, J. Xie and G. Diao, *Electrochem. Acta*, 2014, **136**, 301-309.
35. T. J. Volz, G. R. Hanson and A. E. Fleckenstein, *J. Neurosci. Methods.*, 2006, **155**, 109-115.
36. P. C. Nien, P. Y. Chen and K. C. Ho, *Sens. Actuators, B*, 2009, **140**, 58-64.
37. A. J. Bard and L. R. Faulkner, 1980.
38. G. r. Xu, M. l. Xu, J. m. Zhang, S. Kim and Z. U. Bae, *Bioelectrochemistry*, 2008, **72**, 87-93.
39. S. Li, J. He, M. Zhang, R. Zhang, X. Lv, S. Li and H. Pang, *Electrochem. Acta*, 2013, **102**, 58-65.
40. Y.-R. Kim, S. Bong, Y. J. Kang, Y. Yang, R. K. Mahajan, J. S. Kim and H. Kim, *Biosens. Bioelectron.*, 2010, **25**, 2366-2369.
41. R.Suresh, K.Girbabu, R.Manigandan, S. P. Kumar, S.Munusamy, S.Muthamizh, A.Stephen and V.Narayanan, *Sens. Actuators, B*, 2014, **202**, 440-447.
42. F. Gao, X. Cai, X. Wang, C. Gao, S. Liu, F. Gao and Q. Wang, *Sens. Actuators, B*, 2013, **186**, 380-387.
43. W. Zhu, T. Chen, X. Ma, H. Ma and S. Chen, *Colloids. Surf., B*, 2013, **111**, 321-326.
44. M. Wei, C. Terashima, M. Lv, A. Fujishima and Z. Gu, *Chem. Commun.*, 2009, 3624-3626.
45. X. Yu, K. Sheng and G. Shi, *Analyst*, 2014, **139**, 4525-4531.
46. L. Liu, S. Li, L. Liu, D. Deng and N. Xia, *Analyst*, 2012, **137**, 3794-3799.
47. M. Zhang, K. Gong, H. Zhang and L. Mao, *Biosens. Bioelectron.*, 2005, **20**, 1270-1276.
48. S. C. Fernandes, I. C. Vieira, R. A. Peralta and A. Neves, *Electrochem. Acta*, 2010, **55**, 7152-7157.
49. Z. Guo, M. L. Seol, M. s. Kim, J. H. Ahn, Y. K. Choi, J. H. Liu and X. J. Huang, *Analyst*, 2013, **138**, 2683-26